(Received 30 January 2025, Accepted 10 April 2025, Scheduled 8 May 2025)

Design of a Compact Sub-6 GHz Wideband Filtering Patch Antenna without Extra Structure

Noor K. Mohsin and Dhirgham K. Naji*

The Department of Electronic and Communications Engineering, College of Engineering, Al-Nahrain University, Baghdad, Iraq

ABSTRACT: This paper presents a new compact filtering patch antenna (FPA) design that achieves a wideband impedance bandwidth (IBW) without extra structure. It addresses the limitations of traditional FPAs, which often rely on extra elements to enhance bandwidth and filtering performance. The proposed FPA consists of a radiating patch with an inscribed circular slot, excited by a feedline integrated with a quarter-wavelength matching stripline, all located on the top side of an FR4 substrate. A partial ground plane with a T-shaped symmetrical branch strip is printed on the bottom side of the substrate. The combination of T-shaped strips and the matching stripline creates the first radiation-null f_{n1} near the lower edge of the passband antenna's gain response. Furthermore, the introduction of a circular slot into the radiating patch creates a second radiation-null f_{n2} in the upper edge of the passband region. This not only enhances the IBW but also contributes to the antenna's efficient filtering characteristics. Simulation tools CST Microwave Studio (MWS) and High-Frequency Structure Simulator (HFSS) are used to evaluate key performance parameters, including reflection coefficient (s_{11}), realized gain, and radiation patterns. A fabricated prototype validates these simulations, demonstrating a -10 dB fractional IBW of 47.36% (2.9–4.7 GHz). Based on CST and HFSS simulation results, the design exhibits high selectivity with suppression levels of over 22 dB and 23.7 dB at the lower and upper stopband edges, respectively, while maintaining a flat gain across the passband. The antenna also provides omnidirectional radiation patterns and has a compact size of $29 \times 35 \times 0.8\,\text{mm}^3$, making it more promising for 5G sub-6 GHz applications.

1. INTRODUCTION

Advancement in antenna technology, especially in wideband filtering antennas, can be attributed to the fact that individuals need better ways of communication using less space. With wireless communication technology advancing every day, there is a greater need for wideband filtering antennas nowadays. This is because as most of the wireless communication frequencies head towards higher sides with some specific bands such as sub 6 GHz, it is required that antennas are able to operate on different bands effectively and still provide good performance [1]. Wideband antennas have been created to cover broad frequency spectrums, hence being very appropriate for the fifth generation (5G) systems and internet of things (IoT) equipment. Many times, the design of wideband antennas falls short because they defy the essence of the concept. Nonetheless, portable devices require compact, low-profile antennas due to space constraints. For frequencies below 6 GHz, profile filtering antennas are particularly suitable, as they provide effective filtering without the need for additional physical structures [2]. As modern users increasingly prefer smaller devices, maintaining high performance remains essential. Notably, filtering antenna is efficiently designed to achieve a compact size, enhance boresight gain, and improve frequency response [3].

So it is vital to note the proposed filtering antenna design that does not require extra components [4]. The creation of radiation nulls in the gain response using some innovation design methodologies has led to the introduction of these approaches, such as parasitic patch implementation [5], integration of short circuit probe [6], metasurface design [7], circular/rectangular patch [8], and slot loaded patch [9] among others. These techniques improve the antenna's filtering capability. The integration of antenna and filters has gained popularity in antenna design research. This is because it is possible to reduce the sizes, losses, and costs of radio frequency (RF) front ends while enhancing overall system performance through the combination of a filter's characteristic and an antenna radiation property simultaneously [10–20]. If the radiation nulls' frequency can be manipulated through changing certain properties of the adjacent design, one is able to have control of the passband around particular frequency requirements and make it variable too. In order to achieve wider bandwidth, it is usual to incorporate some strategies like having air layer or multilayer structures, but they lead to higher antenna profiles [21].

In the fulfillment of LTE and 5G spectrum needs, data rates will increase; more information will be accommodated; and there will be many uses possible in all areas such as consumer, industry, as well as safety communication at between 2.8 GHz and 4.9 GHz. It will be important to provide future wireless networks with advanced features to take advantage of this frequency band as 5G deployments progress. The use of LTE (Long Term Evolution) and WiMAX applications within the 5G frequency spectrum especially from 2.8 GHz to 4.9 GHz have many applications which have been enabled by

* Corresponding author: Dhirgham Kamal Naji (dhurgham.kamal.1@nahrain-univ.edu.iq).

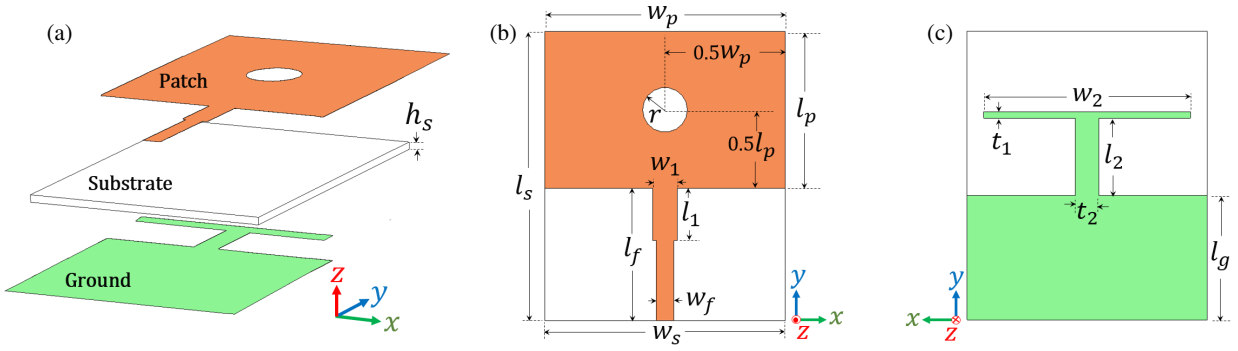

FIGURE 1. Configuration of the proposed filtering antenna. (a) 3D view. (b) Top view. (c) Bottom view.

these frequencies. Some of these applications are Enhanced Mobile Broadband (eMBB), Ultra-Reliable Low Latency communication (URLLC), Massive Machine Type Communication (mMTC), and Fixed Wireless Access (FWA). The aforementioned 5G and LTE bands can be summarized as [22]

- 2.8 GHz–4.2 GHz: This range is closely related to the extended LTE bands such as n77/n78 (5G), and it is often used for offering services in mobile broadband communication system also WiMAX at 3.5 GHz.
- 4.4 GHz to 4.9 GHz: LTE (n79) and 5G can benefit from these frequencies as they provide increased capacity, lower latency, and support more users/devices.

Recently, new types of adopted techniques have been employed in filtering antenna designs to satisfy the aforementioned 5G and LTE bands. For instance, [23] introduced a miniaturized wideband filtering metasurface antenna with a 3×3 metasurface and driven patch. Symmetrically arranged shorting vias and an open stub generate radiation nulls in the lower and upper stopbands. Another filtering method is proposed in [24], which is characterized by a wideband end-fire filtering antenna with driven elements, parasitic strips, a U-shaped ground, and directors to improve both bandwidth and radiation performance. Additionally, a compact, low-profile filtering antenna with mirror-symmetric shorted patches and differential feeding achieves reduced cross-polarization, enhanced bandwidth, and improved gain, as presented in [25]. Multiple slots are incorporated to simultaneously improve IBW and selectivity. The concept of using two differently sized U-slots to generate two independently adjustable radiation nulls by integrating the filtering function with a patch antenna was proposed in [26]. This design results in a sharp band skirt and enhanced selectivity in the boresight gain response.

Furthermore, a novel design proposed in [27] functions as a third-order filter with two constrained radiation nulls outside the passband. It is based on investigating a coaxial-feed filtering patch antenna with parasitic stubs and a transverse path, achieving enhanced filtering performance. In addition, a wideband filtering dipole with tunable radiation nulls is proposed in [28]. It comprises a planar dipole and a microstrip–slotline cross-junction feeding network. By incorporating an open-circuit fed-transmission-line into the extended microstrip feed line, the antenna achieves two radiation nulls in the lower and upper stopbands. An innovative fusion-based method was introduced in [29] for designing a compact, low-profile wideband filtering antenna. Two radiation nulls are simultaneously introduced to both sides of the passband in the antenna's gain by adding inverted Y-shaped symmetrical branches to a traditional semicircle-shaped wide-slot antenna. Additionally, another fusion design of a filtering patch antenna in [30] consists of a radiating patch, ground plane, two pairs of etched slots, and shorted vias. It features a boresight filtering response with gain nulls in the transition bands. Although these designs exhibit good filtering performance, they are based on multilayer configurations, with or without air layers, resulting in tall profiles.

In summary, designing a new filtering antenna with effective harmonic suppression and high performance — characterized by features such as a low profile, enhanced bandwidth, and compact size — remains a challenging task that requires further research and attention. So, this paper presents a new design method of a compact filtering patch antenna (FPA) with a high frequency selectively and enhanced bandwidth without extra filter structure. Two radiation nulls were embedded in the gain response through three techniques: (1) a T-shaped strip branch, (2) a quarter-wave impedance-matching stripline, and (3) a circular slot, aimed at enhancing the filter characteristics. We conducted a detailed investigation into the creation of these nulls and their role in improving overall filtering effectiveness. The antenna prototype is fabricated, and the measured results are compared with the simulated results to verify the design's performance.

2. FILTERING PATCH ANTENNA DESIGN

2.1. Filtering Antenna Configuration

Figure 1 presents the configuration and detailed dimensions of the proposed filtering patch antenna (FPA). As shown in Fig. 1(a), the FPA consists primarily of two layers: patch layer and ground plane layer, which are printed on the top and bottom surfaces of the substrate, respectively. As illustrated in Fig. 1(b), the patch layer comprises a primary rectangular patch with size $w_p \times l_p$, with a circular slot of radius r centered within it. The lower edge of the patch is connected to a 50 Ω microstrip-fed line of length l_f and width w_f, which is integrated with a quarter-wave impedance matching stripline hav-

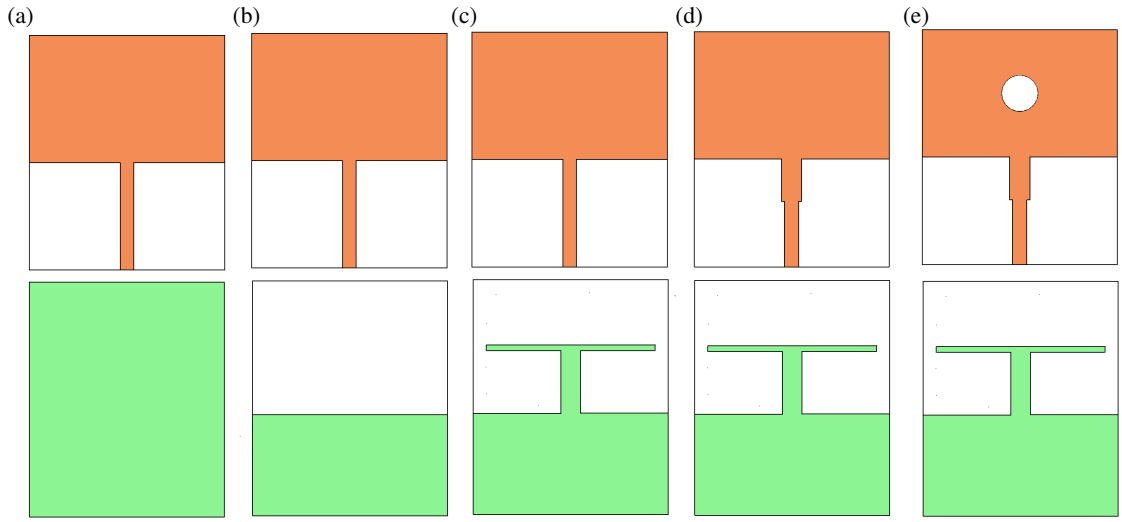

FIGURE 2. Design evolution of proposed antennas, first row is a front side and the second row is a back view: (a) Ant. 1; (b) Ant. 2; (c) Ant. 3; (d) Ant. 4; (e) Ant. 5.

ing dimensions $w_1 \times l_1$. The ground plane layer, illustrated in Fig. 1(c), comprises two sections: a partial ground with a length of l_g and a symmetrical T-shaped strip. The T-shaped strip includes vertical and horizontal components, with dimensions $l_2 \times t_2$ and $w_2 \times t_1$, respectively. The patch and ground layers are printed on an FR4 substrate with overall size $W_s \times L_s$ with thickness $h_s = 0.8\,\text{mm}$, relative permittivity ε_r of 4.33, and loss tangent $\tan\delta$ of 0.02.

A $\lambda_0/4$ impedance transformer is primarily utilized to enhance the antenna's impedance matching. Additionally, the T-shaped arm and circular slot are ultimately useful in precisely positioning two radiation nulls at the lower and upper edges of the antenna's passband gain response. As a result, the proposed FPA is compact, with dimensions $W_s \times L_s = 29 \times 35\,\text{mm}^2$, and achieves a filtering response without the need for any additional filter structures. The optimized dimension parameters of the antenna are detailed in Table 1.

TABLE 1. Optimized dimensions of the proposed FPA.

Parameter	Value (mm)	Parameter	Value (mm)
W_s	29	L_s	35
w_p	29	l_p	19
w_f	2	l_f	16
w_1	3	w_2	25
l_1	6.7	l_2	9.4
t_1	0.8	t_2	2.8
r	2.7	l_g	15
h_s	0.8		

2.2. Design Analysis

This section details the step-by-step process for designing the filtering antenna with the specified characteristics: resonance frequency $f_r = 3.5\,\text{GHz}$, substrate height $h_s = 0.8\,\text{mm}$, dielectric constant $\varepsilon_r = 4.3$, and loss tangent $\tan\delta = 0.02$. The proposed design process was applied to a rectangular microstrip patch antenna (RMPA) to be developed to produce the FPA. Fig. 2 illustrates the five evolutionary design steps, starting from the RMPA in step 1 and ending by the FPA in step 5. The optimal dimensions of the proposed filtering antenna are summarized in Table 1. Fig. 3 presents the plots of the reflection coefficient s_{11}, gain, and efficiency. Performance parameters including: resonance frequency, f_r, reflection coefficient s_{11} at f_r, $s_{11_{|f_r}}$, $-10\,\text{dB}$-impedance bandwidth IBW, first/second radiation nulls in the gain response, f_{n1}/f_{n2}, and gain at f_{n1}/f_{n2}, $G_{|f_{n1}/f_{n2}}$ for the different steps of evolved FPA are summarized in Table 2. These five design steps are described in details as follows.

1) *Step* 1: Design a conventional RMPA. Fig. 2(a) illustrates an RMPA named Ant. 1. The patch width (w_p) and length (l_p) are two important geometrical parameters which depend on the design specifications including ε_r, f_r, and h_s of the antenna under consideration. As stated before, the intended frequency of operation $f_r = 3.5\,\text{GHz}$ is considered, which lies at the middle of the WiMAX band (3.3–3.7 GHz). FR4 material with $\varepsilon_r = 4.3$ and $h_s = 0.8\,\text{mm}$ was used as a substrate. By taking into account these values, the patch dimensions l_p and w_p for the dominant TM_{010} mode can be estimated by using Eqs. (1)–(4) [31]

$$l_p = \frac{v_0}{2f_r\sqrt{\varepsilon_{eff}}} - 2\Delta l_p \tag{1}$$

$$w_p = \frac{v_0}{2f_r\sqrt{(\varepsilon_r+1)/2}} \tag{2}$$

$$\Delta l_p = 0.412h_s\frac{(\varepsilon_{eff}+0.300)}{(\varepsilon_{eff}-0.258)}\frac{((w_p/h_s)+0.262)}{((w_p/h_s)+0.813)} \tag{3}$$

$$\varepsilon_{eff} = \frac{\varepsilon_r+1}{2} + \frac{\varepsilon_r-1}{2}\frac{1}{\sqrt{1+12(h_s/w_p)}} \tag{4}$$

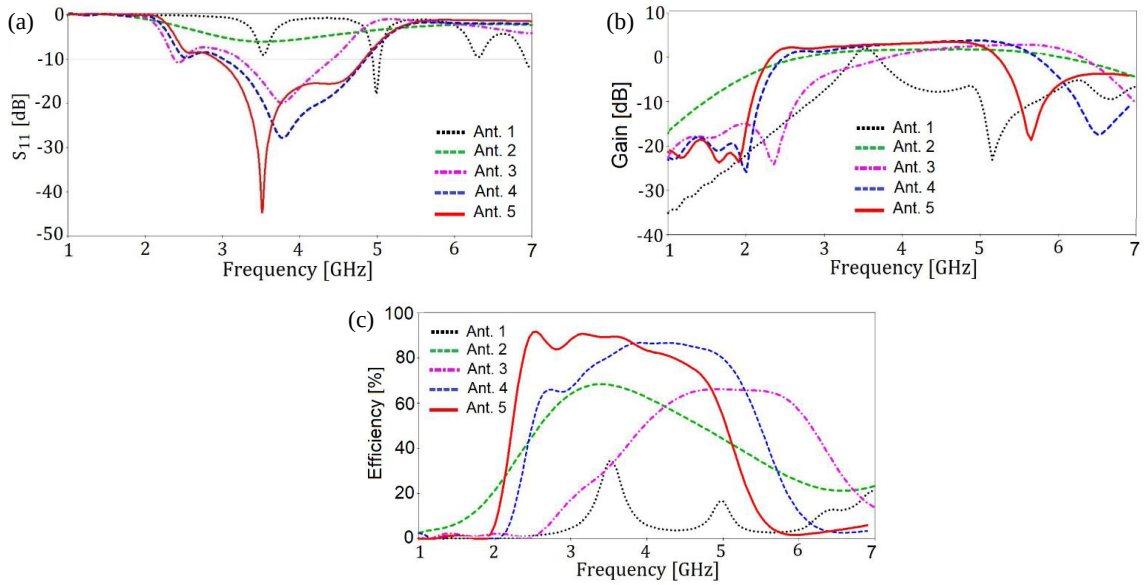

FIGURE 3. Simulated results of five design steps. (a) Reflection coefficients, (b) peak realized gain, and (c) radiation efficiency.

TABLE 2. Performance parameters for the five different steps of evolved FPA.

Design step	f_r (GHz)	$s_{11}\|_{f_r}$ (dB)	−10-dB IBW (GHz)	f_{n1}/f_{n2}	Gain$\|_{f_{n1}/f_{n2}}$	PeakGain (dBi)	Efficiency (%)
Ant. 1	3.51, 4.91, 6.19	−9.5, −18.2, −9.8	N/A, 4.94–5.04, N/A	1.0/5.2	−35.6/−23.5	N/A, 1.4, N/A	N/A, 16.2, N/A
Ant. 2	3.52	−6.4	N/A	1.0/8.0	−17.2/−7	N/A	N/A
Ant. 3	2.40, 3.80	−11.0, −20.2	2.36–2.52, 3.19–4.45	2.3/7.0	−24.6/−10	−15.3, 1.5	1.6 62.8
Ant. 4	2.54, 3.78	−10.0, −28.1	N/A, 3.0–4.9	1.9/6.5	−24.1/−18.6	N/A, 2.9	N/A, 86.4
Ant. 5 (Prop. Ant.)	**2.50** **3.5, 4.4**	**−9.1** **−45, −16**	**N/A** **2.8–4.9**	**2.0/5.8**	**−22.2/−19.6**	**3.0**	**90.4**

where Δl_p, ε_{eff}, and v_0 are the extension of l_p due to the fringing field, the effective dielectric constant of the substrate, and the velocity of light in free space, respectively.

By applying these equations, the geometrical parameters of the conventional RMPA have been calculated as $l_p = 20.52$ mm and $w_p = 26.32$ mm. Then, the RMPA is simulated by employing the full wave electromagnetic Computer Simulation Technology (CST) Microwave Studio (MWS) with the calculated values of l_p and w_p mentioned above as initial dimensions. On the front side of the substrate, a rectangular patch with dimension $w_p \times l_p$ is connected to a 50 Ω SMA connector through the microstrip feedline of length $l_f = 16$ mm and width $w_f = 2$ mm. A complete metallization ground plane is printed on the back side of the substrate. By fine-tuning the antennas' geometrical parameters via CST simulator for resonating at $f_r = 3.5$ GHz, the optimized patch dimensions have been obtained as $l_p = 19$ mm and $w_p = 29$ mm. The total substrate dimensions $W_s \times L_s$ of 29×35 mm^2 are used for the RMPA.

Three resonance frequencies f_{r1}, f_{r2}, and f_{r3} of 3.51, 4.91, and 6.19 GHz corresponding to TM_{010}, TM_{002}, and TM_{020} modes, respectively, are excited by the antenna, as shown in Fig. 3(a). These three resonance frequencies can be calculated by [31]

$$(f_r)_{mnp} = \frac{v_0}{2\pi}\sqrt{\left(\frac{m\pi}{h_s}\right)^2 + \left(\frac{n\pi}{l_p}\right)^2 + \left(\frac{p\pi}{w_p}\right)^2} \quad (5)$$

Substituting in (5), $h_s = 0.8$ mm, $l_p = 19$ mm, and $w_p = 29$ mm, gives the lowest three resonant frequencies (dominant modes), $(f_r)_{010}$, $(f_r)_{002}$, and $(f_r)_{020}$ as 3.8, 5.5, and 7.6 GHz, respectively. This reference antenna serves as the foundation for designing the proposed filtering antenna.

Figures 3(b) and (c) depict the simulated gain and efficiency of the RMPA, shown as dotted black curves. As indicated by this figure and Table 2, the −10-dB IBW is narrow, ranging from 4.94 to 5.14 GHz at $f_{r2} = 4.91$ GHz, with low efficiency 16.2%, peak gain 1.37 dBi, and poor selectivity, characterized

by f_{n1}/f_{n2} (1.0/5.17) in the gain response. Consequently, Ant. 1 fails to demonstrate filtering performance. To achieve a wider frequency band with a filtering response, modifications to Ant. 1 will be implemented to address these shortcomings.

2) *Step* 2: Introducing a partial ground plane. In the second step, Ant. 2 as shown in Fig. 2(b), is evolved from Ant. 1 by replacing its full ground plane of length $l_g = 35$ mm by a partial ground of length $l_g = 15$ mm, which is printed on the back side of the substrate. In this and subsequent steps, all antennas feature an overall size of $29 \times 35\,\text{mm}^2$, with dimensions of $l_g = 15$ mm, $l_f = 16$ mm, and $w_f = 2$ mm. As depicted in Fig. 3(a), Ant. 2 exhibits a poorer reflection coefficient of -6.4 dB at $f_r = 3.52$ GHz, with an unavailable -10-dB IBW. Thus, Ant. 2 requires further modification to achieve the desired filtering response and wider bandwidth.

3) *Step* 3: Employing a symmetrical T-shaped branch strip. To enhance the feature of filtering response, Ant. 3 is designed by adding a symmetrical T-shaped branch strip to the ground of Ant. 2. The branch dimensions are $l_2 \times t_2$ (vertical strip) and $w_2 \times t_1$ (horizontal strip), see Fig. 2(c). As depicted in Fig. 3(a) (dotted-dashed pink curve), Ant. 3 exhibits two -10 dB impedance bandwidths (IBWs): the lower band (2.36–2.52 GHz) with a resonance frequency f_r at 2.4 GHz and the higher band (3.19–4.45 GHz) with $f_r = 3.8$ GHz. Moreover, improved selectivity and better out-of-band suppression are observed at the lower edge of the gain and efficiency responses, achieved by generating the first radiation-null f_{n1} at approximately 2.3 GHz, as shown in Figs. 3(b) and (c). The addition of a T-shaped strip to the ground plane results in enhanced bandwidth and a flatter filtering response, particularly in the lower frequency region. However, further design steps are needed to improve the antenna's filtering capability by introducing a second radiation-null f_{n2} at the upper operational band edge.

4) *Step* 4: Adding a quarter-wave stripline. To improve the antenna's impedance matching and filtering performance, a quarter-wave strip with dimensions $w_1 \times l_1$ is integrated into the feedline of Ant. 3, resulting in the configuration of Ant. 4, as illustrated in Fig. 2(d). It can be observed from Fig. 3(a), blue dashed plot, that Ant. 4 has good impedance bandwidth performance ranging from 3.0 to 4.9 GHz. In addition, as shown in Fig. 3(b), two radiation nulls are generated in the gain response: one at 1.9 GHz and the other at 6.5 GHz. At these frequencies, the antenna's gain decreases significantly, from 10 dBi to -18.6 dBi, enabling effective filtering action for both the upper and lower stop bands. The maximum radiation efficiency, as illustrated in Fig. 3(c), is approximately 86% at the resonance frequency of 3.8 GHz.

However, the suggested modifications to enhance performance characteristics are insufficient, necessitating a final design iteration (Step 5). This step will focus on improving antenna gain, bandwidth, and radiation suppression, as well as refining nulling properties.

5) *Step* 5: Inserting a circular slot within the patch. The final design step involves introducing a circular slot with radius r at the center of the patch of Ant. 4, resulting in Ant. 5, which represents the proposed filtering patch antenna (FPA) design, as shown in Fig. 2(e). This modification enables the antenna to operate at two adjacent resonance frequencies: 3.51 GHz and 4.4 GHz, with corresponding reflection coefficient levels of 44.9 dB and 16 dB, respectively, as illustrated by the red solid curve in Fig. 3(e). Consequently, the antenna achieves a wide 10 dB IBW spanning from 2.8 GHz to 4.9 GHz. The addition of the circular slot enhances the antenna's impedance bandwidth and introduces high selectivity at the upper band edge, delivering a flat passband response, as shown in Fig. 3(b). Within the passband, the antenna exhibits a maximum gain of approximately 3 dBi, along with significant out-of-band suppression ranging from -22.2 dBi to -19.6 dBi at the lower and upper radiation nulls, located at 2 GHz and 5.8 GHz, respectively. As observed in Fig. 3(c), the radiation efficiency within the passband region fluctuates between 70% and 90%.

In summary, the two radiation nulls in the antenna's gain response are achieved through three design techniques: (1) the implementation of a symmetrical T-shaped branch strip in the ground plane, (2) the integration of a quarter-wave stripline within the feedline, and (3) the insertion of a circular slot within the patch. This approach eliminates the need for additional filtering structures, resulting in a compact design suitable for the use in LTE bands such as n77, n78, and n79 (sub-6 GHz 5G), as well as in WiMAX applications at 3.5 GHz.

3. PARAMETRIC STUDY AND WORKING PRINCIPLE

3.1. Parametric Study

The filtering performance of the proposed antenna, defined by the reflection coefficient s_{11} and gain, is predominantly influenced by the radius of the circular slot (r) and the length (l_2) of the T-shaped strip. For understanding the antenna's operation principle, this section presents a detailed analysis of how these critical parameters affect its performance. The simulated s_{11} and peak realized gains for varying values of r and l_2 are illustrated in Figs. 4 and 5, while Tables 3 and 4, respectively, summarize the effects of these variations on the upper and lower radiation nulls as well as the resonance frequencies.

It is clear from Figs. 4(a) and 5(a) that there are three resonance frequencies, f_{r1}, f_{r2}, and f_{r3} which are affected by variations in r and l_2, respectively. In Fig. 4(a), as r rises from 0.7 to 4.7 mm, f_{r1} (f_{r2}) drops from 2.6 (3.75) to 2.4 GHz (3.08 GHz), while f_{r3} alters between 4.43 and 4.62 GHz.

Additionally, as r increases, the magnitude of s_{11} at f_{r1} (f_{r2}), $s_{11_{|f_{r1}}}$ $(s_{11_{|f_{r3}}})$ decreases (increases) from -8.1 (-20.6) to -29.1 dB $(-11.5$ dB), while $s_{11_{|f_{r2}}}$ fluctuates between -25.0 and -38.9 dB. As noticed in Fig. 4(b), when r increases, the first radiation null f_{n1} stays essentially unaltered at ~ 2 GHz, while f_{n2} rises from 5.66 to 6.66 GHz. Thus, the frequency of the upper radiation null can be easily adjusted by varying the parameter r.

Similarly, from Fig. 5(a), it can be observed that as l_2 increases from 7.4 mm to 11.4 mm in increments of 1 mm, both f_{r1} and f_{r2} shift to lower frequency ranges, while f_{r3} moves to a higher frequency region. Additionally, the reflection coefficient s_{11} at f_{r1} (f_{r3}), $s_{11_{|f_{r1}}}$ $(s_{11_{|f_{r3}}})$, decreases (increases) whereas s_{11} at f_{r2} is altered between -21.8 and -44.9 dB. Meanwhile, it can be seen from Fig. 5(b) that the lower (up-

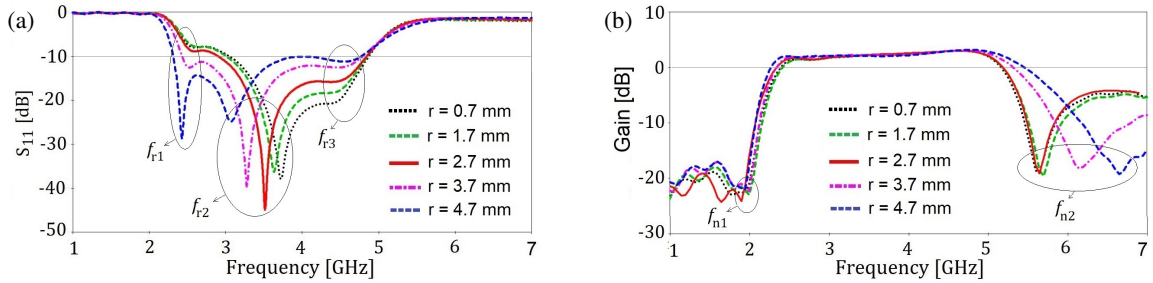

FIGURE 4. Simulated (a) $|s_{11}|$ and (b) peak realized gain of the filtering antenna for different radius of r.

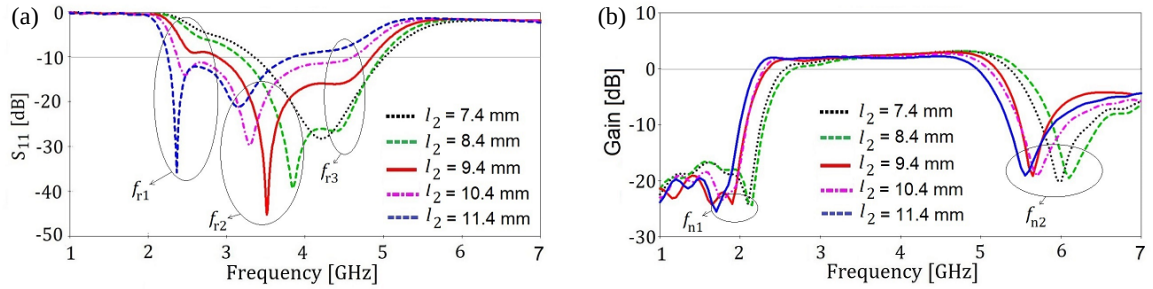

FIGURE 5. Simulated (a) $|s_{11}|$ and (b) peak realized gain of the filtering antenna for different lengths of l_2.

TABLE 3. The impact of varying the radius of circular slot r on the upper and lower radiation nulls as well as the resonance frequencies.

Parameter	Value (mm)	f_r (GHz)	$s_{11}{}_{\lvert f_r}$ (dB)	f_{n1}/f_{n2}	Gain$_{\lvert f_{n1}/f_{n2}}$
r	0.7	2.57, 3.73, 4.43,	−8.1, −38.9, −20.6,	2/6.66	−22.2/−19.4
	1.7	2.6, 3.65, 4.46	−8.0, −36.6, −18.0	2/5.93	−23/−19.5
	2.7	**2.50**, **3.5**, **4.4**	**−9.1**, **−44.9**, **−16.0**	**2/5.85**	**−24.0/−19.5**
	3.7	2.52, 3.3, 4.51	−13.4, −39.8, −12.8	2/6.20	−22.3/−18.0
	4.7	2.4, 3.08 4.62	−29.1, −24.97, −11.45	2/6.66	−22.2/−19.4

per) null frequency f_{n1} (f_{n2}) is lightly (largely) affected as l_2 is allowed to be varied. Therefore, l_2 primarily influences the radiation characteristics across the entire frequency band. In summary, adjusting r and l_2 provides an effective method for tuning the working frequency band, while the radiation nulls can be easily manipulated to enhance filtering performance.

3.2. Working Principle

To further clarify the working principle of the filtering antenna's performance, this section provides a detailed explanation of the mechanism behind the generation of radiation nulls at the lower and upper edges of the passband. Fig. 6 presents the simulated current distribution of the proposed antenna, providing insight into the presence of two radiation nulls, f_{n1} at 2 GHz and f_{n2} at 5.86 GHz.

As shown in Fig. 6(a), at the lower radiation null, specifically at $f_{n1} = 2$ GHz, the current distribution is primarily concentrated along the feedline, the quarter-wave impedance matching stripline, and the edge of the lower half of the circular slot. Additionally, the current flows in the opposite direction along the upper edge of the T-shaped strip. This opposing current flow results in a lower radiation null at f_{n1} due to the path-reversed

TABLE 4. The impact of varying the length's value l_2 on the upper and lower radiation nulls as well as the resonance frequencies.

Parameter	Value (mm)	f_r (GHz)	$s_{11}{}_{\lvert f_r}$ (dB)	f_{n1}/f_{n2}	Gain$_{\lvert f_{n1}/f_{n2}}$
l_2	7.4	N/A, 2.82, 4.21	−5.3, −28.1	2.1/6.0	−24.3/−20.1
	8.4	2.67, 3.85, 4.4	−6.0, −39.0, −26.54	2.1/6.1	−24.3/−19.5
	9.4	**2.50, 3.5, 4.4**	**−9.1, −44.9, −16.0**	**2/5.85**	**−24.0/−19.5**
	10.4	2.47, 3.3, 4.51	−13.9, −29.5, −11.0	1.75/5.7	−23.4/−19.0
	11.4	2.36, 3.2, 4.45	−35.4, −21.8, −8.4	1.7/5.56	−25.5/−18.3

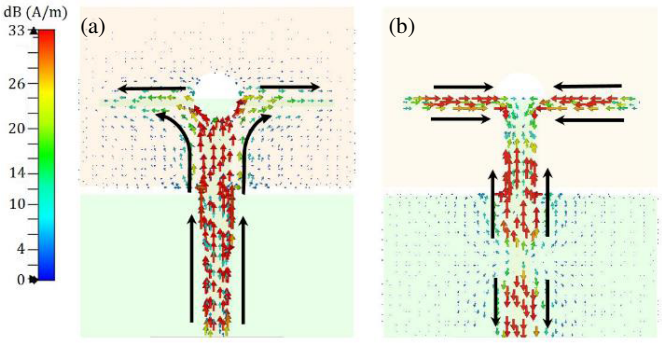

FIGURE 6. Simulated surface current distributions at (a) 2, and (b) 5.85 GHz.

currents canceling each other at the horizontal branch of the T-shaped strip. Fig. 6(b) illustrates that when the antenna operates at the frequency of the upper radiation null ($f_{n2} = 5.85$ GHz), opposite currents are observed on the T-shaped strip. This results in destructive interference, which significantly reduces radiation.

Additionally, the outflow current on the lower edge of the feedline and the inflow current on the quarter-wave transformer flow in opposite directions, further enhancing the destructive interference. Consequently, the radiation null in the high-frequency band is caused by the reverse currents between the upper branch of the T-shaped strip and the opposing currents between the feedline and the quarter-wave transformer. Based on this analysis, it can be concluded that the interaction of reverse currents leads to radiation cancelation, resulting in the two radiation nulls required for the antenna's filtering function.

4. SIMULATED AND MEASURED RESULTS

To validate the CST simulation results of the designed antenna, a 3D simulation tool HFSS is employed to verify antenna's parameters such as the reflection coefficient (s_{11}), realized gain, and radiation patterns.

The prototype of the antenna is then fabricated and tested for its s_{11} performance by vector network analyzer. Photographs of the fabricated antenna along with the measurement setup are shown in Fig. 7.

4.1. Reflection Coefficients

The simulated reflection coefficient s_{11} results from CST MWS and HFSS, along with the corresponding measured result, are presented in Fig. 8. The simulated and measured resonance frequencies (f_r) and −10-dB impedance bandwidths (IBWs) are summarized in Table 5. It can be observed from Fig. 8 and Table 5 that the measured −10-dB IBW is 47.36% (2.9–4.7 GHz) with On the other hand, the −10-dB IBW from CST MWS (HFSS) is 54.54% from 2.8 to 4.9 GHz (74.13% from 2.25 to 4.9 GHz) along with f_{r1} and f_{r2} of 3.5 GHz and 4.4 GHz (3.5 GHz and 4.8 GHz), respectively. These results demonstrate reasonable agreement between the measured and simulated data, with acceptable discrepancies attributed to differences in numerical methods used by the simulators, fabrication tolerances, and measurement calibration.

TABLE 5. The measured results and CST MWS and HFSS simulated results including resonance frequency (f_r) and −10-dB impedance bandwidth (IBW).

Performance Parameters	CST MWS	HFSS	Measurement
−10-dB IBW (GHz)	2.8–4.9	2.25–4.9	2.9–4.7
f_r (GHz)	3.5, 4.4	3.5, 4.8	3.4, 4.3

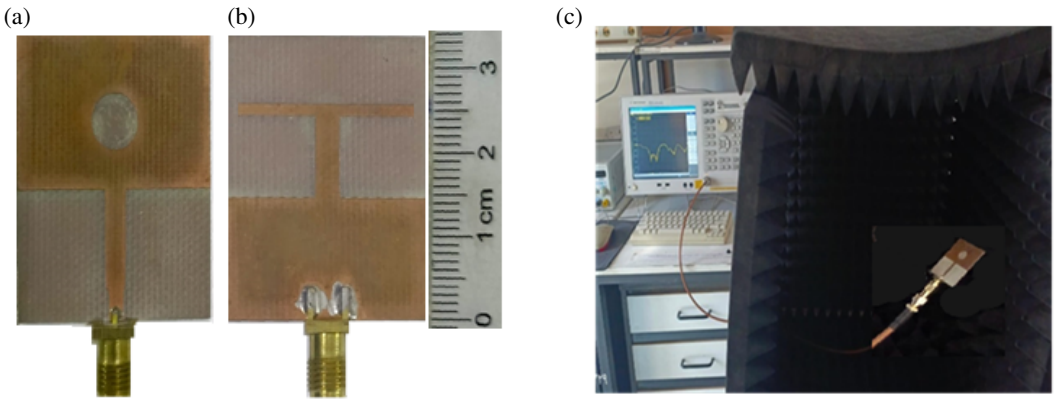

FIGURE 7. Photographs of the fabricated antenna for (a) front side, (b) back side, (c) antenna under measurement.

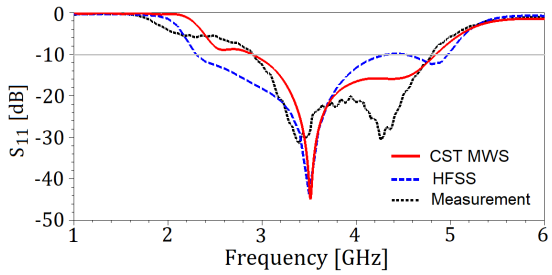

FIGURE 8. Simulated and measured reflection coefficients.

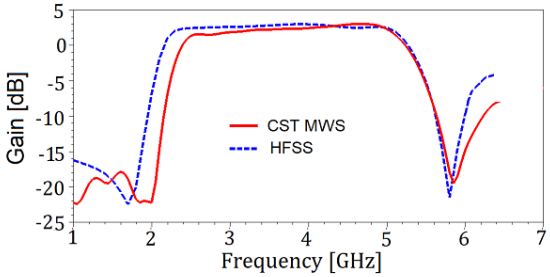

FIGURE 9. The CST and HFSS simulated realized gains of the proposed antenna.

4.2. Realized Gains

Figure 9 shows the CST MWS and HFSS simulated realized gains against frequency of the proposed FPA. Table 6 illustrates these results in terms of the ratio of the first to second radiation nulls f_{n1}/f_{n2}, the gain at the first to the second radiation nulls $\text{Gain}|_{f_{n1}/f_{n2}}$, and the peak gain in the passband. As Fig. 9 and Table 6 show, the CST MWS (HFSS) simulated value of f_{n1}/f_{n2} is 2.0/5.85 (1.7/5.8), while the corresponding $\text{Gain}|_{f_{n1}/f_{n2}}$ value is $-22.2/-19.6$ ($-23.5/-12.6$), demonstrating a nearly flat gain within the passband and a peak gain of 3.0 dBi (2.85 dBi). These results indicate that the proposed antenna exhibits high selectivity with effective out-of-band suppression.

TABLE 6. CST MWS and HFSS simulated peak gain of the FPA.

Simulator	f_{n1}/f_{n2}	$\text{Gain}\|_{f_{n1}/f_{n2}}$	PeakGain (dBi)
CST MWS	2.0/5.85	$-22.2/-19.6$	3.0
HFSS	1.7/5.8	$-23.5/-21.6$	2.85

4.3. Radiation Patterns

To demonstrate the effectiveness of the proposed antenna for radiation across the entire passband, two antenna's resonance frequencies 3.5 and 4.4 GHz are selected for this purpose. The 3D far-field simulation results at 3.5 and 4.4 GHz from CST and HFSS are shown in Figs. 10(a) and (b), respectively. As observed, the antenna exhibits omnidirectional radiation patterns at the two aforementioned frequencies.

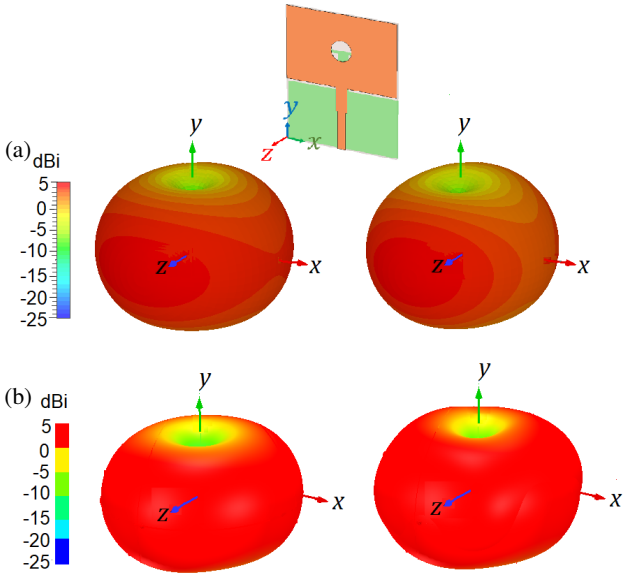

FIGURE 10. The CST and HFSS simulated 2D radiation patterns of the filtering antenna, in the XZ-plane and XY-plane at different frequencies 3.5 GHz and 4.4 GHz: (a) CST MWS and (b) HFSS.

Figure 11 presents the CST and HFSS simulated 2D radiation patterns for the XZ- and XY-planes at 3.5 GHz and 4.4 GHz, respectively. As shown in Fig. 11(a), the antenna exhibits an omnidirectional pattern in the XZ-plane and a bidirectional radiation pattern in the XY-plane when excited at 3.5 GHz. Furthermore, when the antenna is excited at 4.4 GHz,

TABLE 7. Comparisons with reported filtering antennas.

Ref.	Size (mm^2) & (λ_0^2)	Substrate (ε_r/h(mm))	BW (%)	Operating Frequency (GHz)	Peak Gain (dBi)	η %	Extra Filtering structure	No. of layers
[21]	42×43 51×0.53	FR4 $(4.3/1.6)$	54.3	2.63–4.59	6.44	88.9	No	1
[24]	42×43 0.41×0.41	Rogers 4350B $(3.66/3.048, 2, 0.762)$	35.8	3.55–5.12	7.1	92	No	2 + Air
[25]	29×22 0.451×0.342	AD255C $(2.25/1.0)$	14.1	4.34–5.00	5.05	91	No	1
[26]	70×70 0.505×0.505	Rogers 5880 + Air $(2.2, 1/1.57 + 8)$	19.9	2.89–3.53	7.2	NG	No	2 + Air
[27]	30.9×30.9 0.49×0.49	F4B $(2.65/3.0)$	28.0	4.08–5.41	4.92	93	No	1
[28]	44×44 0.52×0.52	Roger 6010 $(10.8/0.635)$	22.4	3.49–4.37	2.7	NG	No	1
[29]	35×29 0.65×0.54	FR4 $(4.4/0.8)$	33.2	4.67–6.53	2	NG	No	1
[30]	85×45 0.85×0.45	Roger RO4003 + Air $(3.55, 1/1.524 + 5)$	3.5	2.9–3.1	6	NG	No	1 + Air
This work	**35×29** **0.41×0.34**	**FR4** **(4.4/0.8)**	**54.5**	**28–49**	**3***	**90.4***	**No**	**1**

Mark (*): indicates the simulated result. NG: Not Given by the original paper.

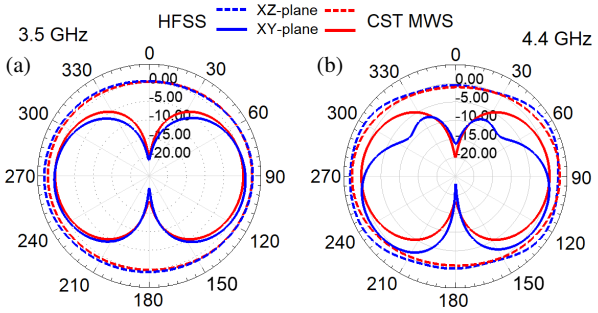

FIGURE 11. The CST and HFSS simulated 2D radiation patterns of the filtering antenna, in the XZ-plane and XY-plane at different frequencies: (a) 3.5 GHz and (b) 4.4 GHz.

it demonstrates a somewhat omnidirectional radiation pattern in the XZ-plane and a slightly distorted bidirectional pattern in the YZ-plane, as observed in Fig. 11(b). These results indicate that the proposed FPA exhibits favorable radiation characteristics.

4.4. Performance Comparisons

To clearly highlight the advantages of the proposed FPA, a performance comparison with recently reported filtering antennas is provided in Table 7. As seen in the table, the design of the present work is simple, with a compact size and no extra structures, while achieving a wide -10 dB fractional IBW compared to others. Additionally, it exhibits a moderate peak realized gain, good radiation efficiency, and high selectivity, attributed to the radiation nulls generated at the lower and upper edges of the passband. The proposed antenna's gain is relatively low compared to some listed antennas but aligns with the average gain of filtering antennas. This is attributed to its low-profile single-layer design, small size, high loss of the FR-4 substrate, and the inherent characteristics of wide-patch antennas. While [23, 26, 30] achieve higher gains with multilayer structures, the proposed antenna excels in balancing low profile, compact size, impedance bandwidth, gain, and frequency selectivity.

5. CONCLUSION

This paper presents a compact, wideband filtering patch antenna (FPA) with a simple design and no additional structures. The antenna exhibits a broad impedance bandwidth, flat gain response within the passband, and high selectivity in the stopband. Thus, the FPA demonstrates an effective filtering response by generating two radiation nulls through the etching of a circular slot in the patch and the addition of a T-shaped strip to the ground plane. To validate the design principle, two simulation software tools, CST MWS and HFSS, are used to extract key antenna performance parameters, including reflection coefficient, realized gain, and radiation patterns. The results from both simulators show good agreement, confirming the accuracy of the simulated results. Afterward, a prototype of the designed antenna is fabricated and measured, to validate the simulated s_{11} result. Experimental result reveals that a -10-dB

IBW of (2.9–4.7 GHz) is exhibited by the antenna. Additionally, the proposed FPA radiates an omnidirectional pattern in XZ-plane and a bidirectional pattern in the XY-plane across the antenna's passband. Due to all of these good features, the proposed filtering antenna is highly promising candidates for 5G Sub-6 GHz wireless applications.

REFERENCES

[1] Al-Yasir, Y. I. A., N. O. Parchin, M. N. Fares, A. Abdulkhaleq, M. S. Bakr, M. Al-Sadoon, J. Kosha, and R. Abd-Alhameed, "A differential-fed dual-polarized high-gain filtering antenna based on SIW technology for 5G applications," in *2020 14th European Conference on Antennas and Propagation (EuCAP)*, 1–5, Copenhagen, Denmark, Mar. 2020.

[2] Andrews, C. J. M., A. S. K. Narayanan, and A. M. Sunil, "Compact metamaterial based antenna for 5G applications," *Results in Engineering*, Vol. 24, 103269, 2024.

[3] Abdul, J., J. U. R. Kazim, M. A. Imran, Q. H. Abbasi, and M. U. Rehman, "Design of a compact ultra-wideband microstrip antenna for millimeter-wave communication," in *2021 IEEE International Symposium on Antennas and Propagation and USNC-URSI Radio Science Meeting (APS/URSI)*, 837–838, Singapore, 2021.

[4] Chen, F.-C., H.-T. Hu, R.-S. Li, Q.-X. Chu, and M. J. Lancaster, "Design of filtering microstrip antenna array with reduced sidelobe level," *IEEE Transactions on Antennas and Propagation*, Vol. 65, No. 2, 903–908, Feb. 2017.

[5] Mao, C.-X., S. Gao, Y. Wang, Z. Wang, F. Qin, B. Sanz-Izquierdo, and Q.-X. Chu, "An integrated filtering antenna array with high selectivity and harmonics suppression," *IEEE Transactions on Microwave Theory and Techniques*, Vol. 64, No. 6, 1798–1805, Jun. 2016.

[6] Dhwaj, K., J. M. Kovitz, H. Tian, L. J. Jiang, and T. Itoh, "Half-mode cavity-based planar filtering antenna with controllable transmission zeroes," *IEEE Antennas and Wireless Propagation Letters*, Vol. 17, No. 5, 833–836, May 2018.

[7] Chu, H. and Y.-X. Guo, "A filtering dual-polarized antenna subarray targeting for base stations in millimeter-wave 5G wireless communications," *IEEE Transactions on Components, Packaging and Manufacturing Technology*, Vol. 7, No. 6, 964–973, Jun. 2017.

[8] Zhang, B. and Q. Xue, "Filtering antenna with high selectivity using multiple coupling paths from source/load to resonators," *IEEE Transactions on Antennas and Propagation*, Vol. 66, No. 8, 4320–4325, Aug. 2018.

[9] Zhang, Y., X. Y. Zhang, and Y.-M. Pan, "Low-profile planar filtering dipole antenna with omnidirectional radiation pattern," *IEEE Transactions on Antennas and Propagation*, Vol. 66, No. 3, 1124–1132, Mar. 2018.

[10] Chen, B.-J., X.-S. Yang, and B.-Z. Wang, "A compact high-selectivity wideband filtering antenna with multipath coupling structure," *IEEE Antennas and Wireless Propagation Letters*, Vol. 21, No. 8, 1654–1658, Aug. 2022.

[11] Xi, L., "A wideband planar filtering dipole antenna for 5G communication applications," *Microwave and Optical Technology Letters*, Vol. 61, No. 12, 2746–2751, 2019.

[12] Cheng, G., B. Huang, Z. Huang, and L. Yang, "A high-gain circularly polarized filtering stacked patch antenna," *IEEE Antennas and Wireless Propagation Letters*, Vol. 22, No. 5, 995–999, May 2023.

[13] Xu, K., J. Shi, X. Qing, and Z. N. Chen, "A substrate integrated cavity backed filtering slot antenna stacked with a patch for frequency selectivity enhancement," *IEEE Antennas and Wireless Propagation Letters*, Vol. 17, No. 10, 1910–1914, Oct. 2018.

[14] Liu, X., K. Ning, S. Xue, L. Ge, K. W. Leung, and J.-F. Mao, "Printed filtering dipole antenna with compact size and high selectivity," *IEEE Transactions on Antennas and Propagation*, Vol. 72, No. 3, 2355–2367, May 2024.

[15] Liang, G.-Z., F.-C. Chen, H. Yuan, K.-R. Xiang, and Q.-X. Chu, "A high selectivity and high efficiency filtering antenna with controllable radiation nulls based on stacked patches," *IEEE Transactions on Antennas and Propagation*, Vol. 70, No. 1, 708–713, Jan. 2022.

[16] Tang, M.-C., D. Li, Y. Wang, K.-Z. Hu, and R. W. Ziolkowski, "Compact, low-profile, linearly and circularly polarized filtennas enabled with custom-designed feed-probe structures," *IEEE Transactions on Antennas and Propagation*, Vol. 68, No. 7, 5247–5256, Jul. 2020.

[17] Li, L., H. D. Xiong, W. Y. Wu, A. B. Fu, and J. Y. Han, "A T-shaped strips loaded wideband filtering patch antenna with high selectivity," *IEEE Antennas and Wireless Propagation Letters*, Vol. 23, No. 1, 89–93, Jan. 2024.

[18] Hu, P. F., Y. M. Pan, X. Y. Zhang, and B.-J. Hu, "A filtering patch antenna with reconfigurable frequency and bandwidth using F-shaped probe," *IEEE Transactions on Antennas and Propagation*, Vol. 67, No. 1, 121–130, Jan. 2019.

[19] Li, D. and C. Deng, "A single-layer filtering antenna with two controllable radiation nulls based on the multimodes of patch and SIW resonators," *IEEE Antennas and Wireless Propagation Letters*, Vol. 22, No. 3, 551–555, Mar. 2023.

[20] Zhang, X. Y., W. Duan, and Y.-M. Pan, "High-gain filtering patch antenna without extra circuit," *IEEE Transactions on Antennas and Propagation*, Vol. 63, No. 12, 5883–5888, Dec. 2015.

[21] Jin, J. Y., S. Liao, and Q. Xue, "Design of filtering-radiating patch antennas with tunable radiation nulls for high selectivity," *IEEE Transactions on Antennas and Propagation*, Vol. 66, No. 4, 2125–2130, Apr. 2018.

[22] Li, J.-F., Z. N. Chen, D.-L. Wu, G. Zhang, and Y.-J. Wu, "Dual-beam filtering patch antennas for wireless communication application," *IEEE Transactions on Antennas and Propagation*, Vol. 66, No. 7, 3730–3734, Jul. 2018.

[23] Li, D., H.-L. Zhou, K.-Z. Hu, Z. Chen, Y. Yu, and D. Yan, "Single-layer wideband and dual-band end-fire filtering antennas with high front-to-back ratio," *IEEE Antennas and Wireless Propagation Letters*, Vol. 24, No. 2, 399–403, Feb. 2025.

[24] Liu, X., K. Ning, S. Xue, L. Ge, K. W. Leung, and J.-F. Mao, "Printed filtering dipole antenna with compact size and high selectivity," *IEEE Transactions on Antennas and Propagation*, Vol. 72, No. 3, 2355–2367, Mar. 2024.

[25] Xiong, X., W. Xue, J. Qi, W. Shang, and W. Li, "Miniaturized wideband metasurface antenna with filtering performance for 5G application," *IEEE Antennas and Wireless Propagation Letters*, Vol. 24, No. 1, 3–7, Jan. 2025.

[26] Li, D., H.-C. Tang, K.-Z. Hu, M.-C. Tang, Z. Chen, and D. Yan, "A compact low-profile single-layer differentially-fed shorted patch filtenna with low cross-polarization," *IEEE Antennas and Wireless Propagation Letters*, Vol. 23, No. 10, 3222–3226, Oct. 2024.

[27] Sung, Y., "Simple patch antenna with filtering function using two U-slots," *Journal of Electromagnetic Engineering and Science*, Vol. 21, No. 5, 425–429, 2021.

[28] Yang, D., H. Zhai, and C. Guo, "A simple filtering patch antenna based on stub-loaded resonator," *Microwave and Optical Tech-*

nology Letters, Vol. 63, No. 7, 1920–1926, Jul. 2021.

[29] Yang, G., M. Li, L. Xiang, R. Xiao, Y. Qian, S. Qi, and W. Wu, "A slotline-fed wideband dipole with filtering gain response," *IET Microwaves, Antennas & Propagation*, Vol. 16, No. 13, 841–845, 2022.

[30] Cheng, G., J. Zhou, B. Huang, L. Yang, and Z. Huang, "Compact low-profile wideband filtering antenna without additional filtering structure," *IEEE Antennas and Wireless Propagation Letters*, Vol. 22, No. 10, 2477–2481, Oct. 2023.

[31] Balanis, C. A., *Antenna Theory: Analysis and Design*, John Wiley & Sons, 2016.